Ideal Energy-Level Alignment at the ZnO/P3HT Photovoltaic Interface

*Keian Noori and Feliciano Giustino**

Hybrid semiconductor-polymer nanostructured solar cells hold the promise of photovoltaic energy conversion based on abundant and nontoxic materials and scalable manufacturing processes. After a decade of intense research activity, hybrid solar cells still exhibit low short-circuit currents and moderate open-circuit voltages. These bottlenecks call for a detailed understanding of the physics underlying the device operation at the nanoscale. Using first-principles calculations the ideal energy-level alignment of hybrid solar cell interfaces based on the wide bandgap semiconductor ZnO and the polymer poly(3-hexylthiophene) (P3HT) is investigated. The interfacial charge transfer is quantified and it is shown that this effect increases the ideal open-circuit voltage with respect to the electron-affinity rule by as much as 0.5 V. The results of this work suggests that there is significant room for optimizing this class of excitonic solar cells by tailoring the semiconductor/polymer interface at the nanoscale.

1. Introduction

Hybrid organic-inorganic nanostructured solar cells based on semiconductor nanocrystals and conducting polymers[1] have emerged as a potential alternative to dye-sensitized and all-organic solar cells. In hybrid solar cells the organic component enables the deposition of the active layer onto flexible substrates, while the inorganic component offers high carrier mobilities and the possibility to enhance photon harvesting by tuning the absorption via quantum size effects.[2] During the past five years hybrid solar cells based on ZnO and poly(3-hexylthiophene) (P3HT) have received considerable attention[3] due to the ease of processing ZnO at low temperatures[4] and the relatively large hole mobility (up to 0.1 $cm^2\ V^{-1}\ s^{-1}$) of P3HT.[5] Between 2006 and 2011 hybrid ZnO/P3HT solar cells using a semiconductor/polymer bilayer,[6–11] quantum dot/polymer blends,[6,12–16] infiltrated nanowire arrays,[6,7,10,17–21] polymer-coated single nanowires,[22] and nanorod/polymer blends[16] have been demonstrated. The power conversion efficiencies of these devices, however, have not exceeded 2% due to low short-circuit currents (<5 mA cm^{-2}) and open-circuit voltages in the range 0.4–0.8 V.[23] While the effects of substrate processing,[10] doping,[8] surface treatment,[11] and polymer morphology[20] on the performance of hybrid ZnO/P3HT solar cells have been investigated in detail, the atomic-scale physics underlying the open-circuit voltage in these devices has not been addressed yet. In this context a detailed understanding of the energy-level alignment at the interface between ZnO and P3HT is critical in order to establish the ideal open-circuit voltage and identify new optimization strategies.

In this work we investigate the electronic energy-level alignment at the ZnO/P3HT interface from first principles. The ground-state atomistic structures of the semiconductor, the polymer, and their interface are described by means of standard density-functional theory (DFT), while the energy-level alignment at the interface is studied using a combined DFT and hybrid-functional approach.[24] We first generate a large atomistic model of the ZnO/P3HT interface using a bilayer geometry. Next, we calculate the energy-level alignment for this interface model and we quantify the effect of interfacial charge transfer on the resulting ideal open-circuit voltage. All computational details are provided in the Computational Methods section.

2. Results and Discussion

2.1. Atomistic Model of the ZnO/P3HT Interface

At ambient conditions ZnO crystallizes in the wurtzite structure. For this structure we calculate the optimized lattice parameters $a = 3.19$ Å and $c = 5.15$ Å, in agreement with measured[25] and calculated[26,27] values. The ground-state structure of crystalline P3HT is determined using a unit cell containing four thiophene rings. Owing to multiple minima in the total energy landscape, we perform structural optimizations starting from three different initial configurations, each with a varying degree of alkyl side chain interdigitation: no interdigitation, interdigitation up to half the length of the alkyl chains, and full interdigitation. After optimization the first two initial configurations exhibit the same partially interdigitated structure, while the latter configuration exhibits a fully interdigitated structure. For these two configurations our calculated interlayer separation $b = 3.81$, 3.85 Å, monomer length along the backbone $c = 7.71$, 7.72 Å, and interdigitation along the side chains $d = 15.9$,

K. Noori, Dr. F. Giustino
Department of Materials
University of Oxford
Parks Road Oxford, OX1 3PK, UK
E-mail: feliciano.giustino@materials.ox.ac.uk

DOI: 10.1002/adfm.201201478

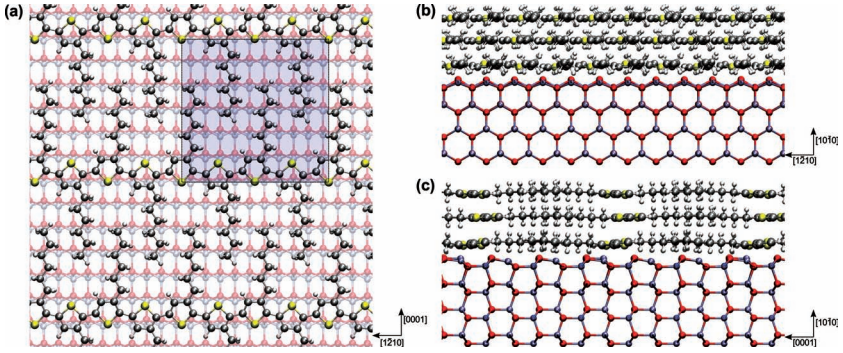

Figure 1. ZnO(10$\bar{1}$0)/P3HT interface model. a) Top view of a single layer of P3HT adsorbed on ZnO, with the two-dimensional periodic unit cell highlighted. b) Side view of the optimized ZnO/P3HT interface model, with the alkyl side chains perpendicular to the page. c) Side view of the ZnO/P3HT interface model, with the polythiophene backbone running perpendicular to the page. The model is composed of 4 layers of ZnO and 3 layers of P3HT. Atomic color code: O (red), Zn (blue), S (yellow), C (grey), and H (white).

13.3 Å, are in good agreement with previous calculations[28–30] and experiment.[31–34] Since thermal vibrations prevent full interdigitation at room temperature,[30] we construct our interface model by using the partially interdigitated configuration.

In order to mimic ZnO/P3HT bilayer devices[6–11] and ZnO/P3HT core-shell nanowires[22] we construct semiconductor/polymer interfaces using a periodic slab geometry where P3HT layers are stacked on top of a ZnO film exposing its (10$\bar{1}$0) surface. The nonpolar (10$\bar{1}$0) surface is chosen since it is the most energetically favorable ZnO termination.[25] Our models contain 4 layers of ZnO and 3 layers of P3HT, totalling 540 atoms and 2880 valence electrons (**Figure 1**). We choose to adopt models where P3HT lamellae lie flat on the ZnO(10$\bar{1}$0) surface based on the findings of Briseno et al.[22] In that study TEM images of ZnO/P3HT core-shell nanowires show multiple layers of the polymer stacked on the ZnO surface. The authors note that this stacking is consistent with the polythiophene backbone running parallel to the ZnO surface. Since the P3HT interlayer separation in the TEM images is similar to our calculated *b* parameter (3.85 Å), it is reasonable to assume that the alkyl chains are oriented parallel to the nanowire surface. This is in line with the study of Dag and Wang,[27] and such a lamellar morphology has also been observed by Sirringhaus et al.[5] and by Kline et al.[35]

We determine the most stable interface morphology by optimizing the geometry of a P3HT monolayer starting from four initial configurations. In each of these configurations the P3HT backbone is aligned either along the [1$\bar{2}$10] or the [0001] direction of ZnO, with the C atoms at the 2,5 sites of the thiophene rings placed either atop or in the trenches between Zn-O dimers. After carrying out structural optimizations we identify the most stable configuration as that with the backbone aligned along the [1$\bar{2}$10] direction and the reference C atoms in the trenches (Figure 1a), in agreement with previous theoretical studies.[27,36] In this configuration the polymer backbone is almost lattice-matched to the ZnO surface, the *c* parameter being only slightly shorter (3%) than in bulk P3HT. Starting from this optimized structure we construct a more realistic model by adding two additional layers of P3HT (Figure 1b,c). In the optimized interface model the P3HT layers develop small ripples along the alkyl side chains (<0.5 Å in the direction perpendicular to the substrate) in order to adapt to the underlying ZnO(10$\bar{1}$0) surface. The polythiophene backbone remains essentially unchanged with respect to bulk P3HT.

2.2. Electronic Structure of the ZnO/P3HT Interface

The calculation of the interfacial energy-level alignment is performed by applying hybrid-functional corrections to the band offsets determined from a DFT calculation at the interface following Alkauskas et al.[24] The corrections to the band edges are evaluated through separate calculations on bulk ZnO and bulk P3HT. In the bulk calculations we first determine the mixing fraction α of Hartree-Fock exchange in such a way as to reproduce experimental band gaps, and then use this value of the mixing parameter for evaluating the hybrid corrections to the band edges. We independently validate this scheme by considering a test interface comprised of a thiophene molecule adsorbed on the ZnO(10$\bar{1}$0) surface[37,38] (see Computational Methods).

Figure 2 shows the valence band maximum (VBM) and conduction band minimum (CBM) of the substrate, and the highest occupied molecular orbital (HOMO) and lowest unoccupied molecular orbital (LUMO) of the polymer. The band extrema thus identified for ZnO and P3HT (**Table 1**) yield gaps within 0.1 eV of the corresponding bulk values, thereby confirming our assignment. The ZnO CBM exhibits Zn 4s and O 2p character, the P3HT HOMO is derived from C π states and the LUMO is of $\pi*$ character. This analysis is consistent with previous calculations.[27] While the HOMO of the polymer is localized on the polythiophene backbone of the second and third P3HT layers, the LUMO is localized on the backbone of the first layer and overlaps significantly with the underlying ZnO substrate (Figure 2). As a result, the interface morphology considered here, wherein the P3HT lamellae lie parallel to the ZnO surface, is expected to lead to a more efficient charge transfer as compared to the alternative edge-on morphology, in which P3HT lamellae are adsorbed perpendicular to the surface.

2.3. Open-Circuit Voltage and Comparison with Experiment

The maximum attainable open-circuit voltage (V_{OC}) of an hybrid ZnO/P3HT solar cell corresponds to the difference between the CBM of ZnO and the HOMO of P3HT. Based on our calculated energy-level alignment, presented in Table 1, we find V_{OC} = 2.07 V for our interface model (**Figure 3**b). Within our error bar of 0.1–0.2 eV (see Computational Methods), this value can be considered to match the optical gap of P3HT (1.9 eV), indicating that the ZnO/P3HT interface is intrinsically capable of operating with a negligible "loss-in-potential".[42]

Table 1 shows that the calculated energy offset between the ZnO CBM and the P3HT LUMO is 0.53 eV. This value

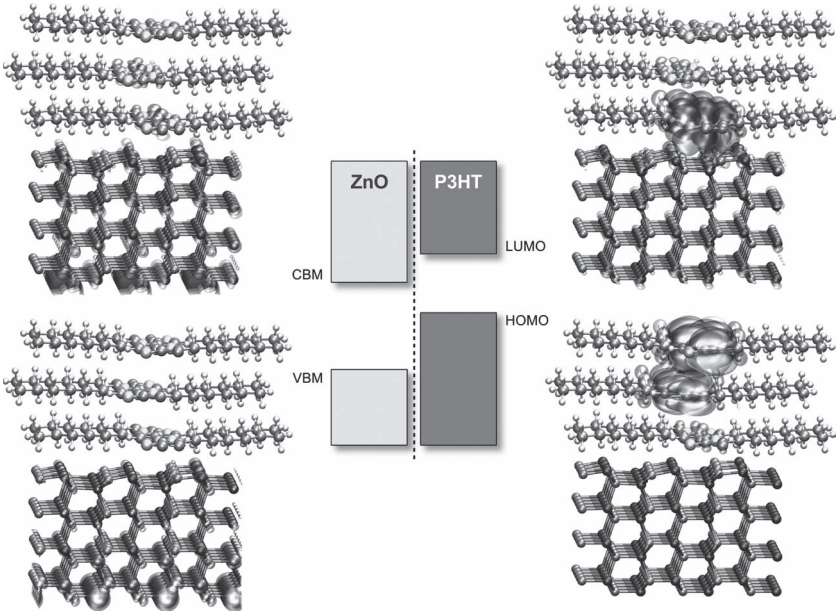

Figure 2. Frontier orbitals and band extrema at the ZnO(10$\bar{1}$0)/P3HT interface. Isosurface plots of the P3HT HOMO and LUMO wavefunctions (isovalue: 6.75×10^{-4} Å^{-3}), calculated for the ZnO(10$\bar{1}$0)/P3HT interface model shown in Figure 1b,c. The proximity of the polymer backbone to the substrate leads to a significant overlap between the P3HT LUMO level and the the ZnO conduction states (upper right corner), thereby favoring the efficient transfer of electrons upon exciton dissociation. A schematic energy-level diagram is included for clarity.

falls within the range 0.4–0.7 eV of exciton binding energies reported for P3HT.[41,43] The energy-level alignment determined here is therefore fully compatible with exciton dissociation at the interface and, in particular, with measurements of the external quantum efficiency showing an onset for charge generation around 1.9–2.0 eV (625–650 nm).[9]

The ideal V_{OC} estimated from measured work functions using the electron affinity rule is 1.6 V.[39,40] In the electron affinity model the interfacial energy diagram is obtained by aligning the vacuum levels of the two materials forming the interface (Figure 3a). In real heterojunctions, however, the charge transfer between donor and acceptor generates a dipole and a corresponding potential offset that acts to reduce the energy mismatch.[44–46]

We quantify this effect by calculating the electronic charge rearrangement upon formation of the interface and the resulting electrostatic potential offset. **Figure 4**a shows that there is significant charge transfer from the first P3HT monolayer to the the first ZnO layer underneath. The total charge transferred from the polymer to the semiconductor is 1.4×10^{13} electrons cm^{-2} (0.075 electrons per thiophene ring), and the associated electrostatic potential offset is calculated to be V_{dip} = 0.5 eV (Figure 4b). We verified this result by comparing the KS energy levels at the ZnO/P3HT interface with those corresponding to the isolated ZnO and P3HT layers (see Computational Methods). This charge transfer goes in the direction of aligning the band edges of the two materials, in agreement with considerations based on the matching of the respective charge neutrality levels.[47] The calculated magnitude of the electrostatic potential offset is comparable with the V_{OC} predicted by the electron affinity rule, therefore the standard approximation of neglecting this effect is inadequate for the ZnO/P3HT interface. If we take the energy diagram obtained from the electron affinity rule and add our calculated interfacial dipole, we obtain a CBM/HOMO separation (i.e., an ideal V_{OC}) of 2.1 V, in good agreement with our first-principles band alignment.

The open-circuit voltage measured in actual devices falls in the range 0.4–0.8 V.[23] Apart from possible non-ideality effects associated with dark current and carrier recombination,[48] it is possible that the difference between ideal and actual open-circuit voltages may relate to conformational disorder in the polymer near the interface, and/or defective ZnO surfaces. In the optical absorption spectrum of P3HT on ZnO, for example, the peak at 560 nm and the low-energy shoulder at 610 nm observed for crystalline P3HT on glass are suppressed, indicating the formation of a disordered P3HT layer at the interface.[49] In addition, ultraviolet photoemission spectroscopy measurements show that the HOMO level of regiorandom

Table 1. Energies of ZnO VBM, CBM and P3HT HOMO, LUMO at the ZnO(10$\bar{1}$0)/P3HT interface. The energy levels under "KS" correspond to the DFT Kohn-Sham states at the interface. In the second column we report the hybrid-functional corrections ΔH to the DFT levels of bulk ZnO and of bulk P3HT (with α_s = 0.375 and α_p = 0.367, respectively). In the third column we give the VBM, CBM, HOMO, and LUMO levels after applying the hybrid-functional corrections to the KS energies. We also report the band gaps at the interface for completeness. The zero of the energy axis is set to the P3HT HOMO level in all cases.

		KS [eV]	ΔH [eV]	Hybrid [eV]
ZnO	CBM	0.07	0.98	2.07
	VBM	–0.64	–1.66	–1.28
	E_g	0.71	2.64	3.35
P3HT	LUMO	0.82	0.76	2.60
	HOMO	0.00	–1.02	0.00
	E_g	0.82	1.78	2.60

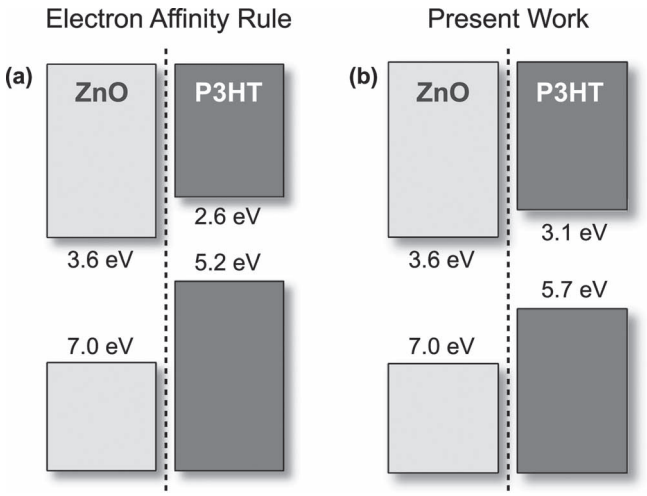

Figure 3. Schematic energy-level alignment at the ZnO/P3HT interface. a) Empirical energy diagram obtained within the electron affinity rule, using the ZnO work function of Gwinneret al.[39] and the P3HT ionization potential and bandgap of Onoda et al.[40] and Deibel et al.[41], respectively. b) Energy-level diagram obtained using our combined density-functional and hybrid-functional calculations based on the interface model in Figure 1b,c. Our calculations include the effects of the interfacial charge transfer, which are neglected in (a). For ease of comparison with the literature the levels in both panels are shifted in order to set the ZnO CBM at 3.6 eV below the vacuum level.

3. Conclusions

In summary, by using a combination of density-functional and hybrid-functional calculations on very large atomistic models, we find that the ZnO/P3HT interface has the potential of delivering open-circuit voltages larger than those estimated using the electron affinity rule. Our calculations highlight the key role of interfacial charge transfer in the energy-level alignment, and call for detailed photoemission studies on ZnO/P3HT interfaces of well controlled morphology. This work will serve as a basis for further investigation into the origin of the low open-circuit voltages measured in actual ZnO/P3HT solar cells, and for developing practical optimization strategies.

4. Computational Methods

Density-Functional Calculations: Density-functional and hybrid-functional calculations were carried out using the Quantum ESPRESSO software package.[52] The core-valence interaction was described by means of ultrasoft pseudopotentials[53] (for structural minimizations) and norm-conserving pseudopotentials[54,55] (for electronic structure calculations). The valence electronic wavefunctions and charge density were described using planewave basis sets with kinetic energy cutoffs of 35 Ry and 320 Ry, respectively, in the case of ultrasoft pseudopotentials, and with a kinetic energy cutoff of 100 Ry in the case of

P3HT is 0.3 eV higher that in regioregular P3HT.[50] Taken together, these results suggest that conformational disorder of P3HT at the interface may reduce V_{OC} by up to 0.3 eV. Furthermore, the presence of oxygen vacancies in ZnO near the interface may pin the the ZnO Fermi level close to the defect levels, similar to the behavior observed in Schottky contacts to ZnO.[51] In particular, the V_O (+2,0) defect level of ZnO lies 0.7 eV below the ZnO CBM,[51] therefore CBM/HOMO offsets and V_{OC} of similar magnitude may be expected.

Our present findings suggest that the low V_{OC}'s reported in the literature are not an intrinsic property of the ZnO/P3HT interface, but must be related to extrinsic effects such as inhomogeneity and defects. By reducing the defect density at the ZnO surface and by increasing polymer crystallinity it should be possible to achieve a substantial increase in the efficiency of ZnO/P3HT solar cells. Indeed, if it were possible to realize an hybrid cell as in the work by Oosterhout et al.[15] with a short-circuit current of 5.2 mA cm^{-2} and a fill factor of 52% (under AM1.5 illumination), but with our calculated open circuit voltage of 2.07 V, then the device efficiency would be as high as 5.6%. This prospect makes the ZnO/P3HT system attractive for technological applications.

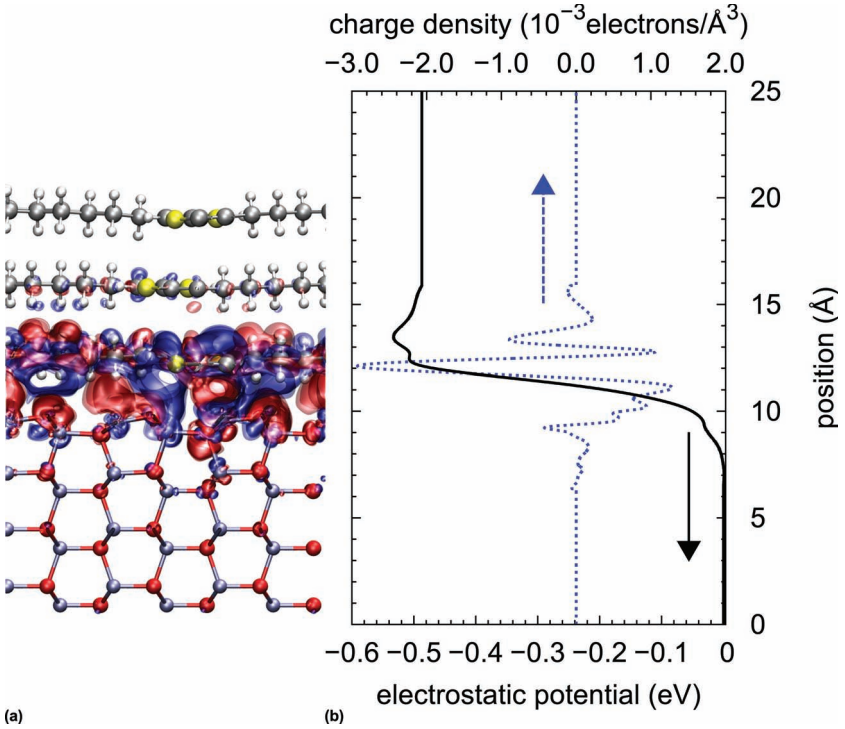

Figure 4. Charge transfer at the ZnO/P3HT interface. a) Isosurface of the charge redistribution upon formation of the interface (isovalue: ±2.02 × 10^{-3} electrons Å^{-3} for red/blue), obtained as $n_{ZnO/P3HT} - [n_{ZnO} + n_{P3HT}]$. $n_{ZnO/P3HT}$, n_{ZnO}, and n_{P3HT} are the electronic charge densities of the interface and the isolated ZnO and P3HT, respectively. b) Planar average of the charge redistribution (dashed blue line) and corresponding electrostatic potential profile across the interface (solid black line), as obtained by integrating Poisson's equation.

norm-conserving pseudopotentials. For structural minimizations the local-density approximation (LDA) to DFT[56,57] was used. While the LDA does not include dispersion forces, it has been shown to yield crystalline structures of P3HT in agreement with experiment,[28] and a physisorption geometry of P3HT on ZnO in agreement with second order Møller-Plesset perturbation methods.[27] The crystal structures of bulk ZnO and bulk P3HT were optimized by sampling the Brillouin Zone (BZ) through $8 \times 8 \times 8$ and $4 \times 4 \times 4$ Monkhorst-Pack grids, respectively. Auxiliary BZ grids of size $4 \times 4 \times 4$ and $2 \times 2 \times 2$ were used for the evaluation of the bare Coulomb term in the hybrid-functional calculations of ZnO and P3HT, respectively. For all the interface models a Γ-point sampling was used. The transverse area of the ZnO slab is 15.93×15.46 Å^2, and periodic replicas of the ZnO/P3HT interface are separated by 9.5 Å of vacuum. During the structural optimization of the ZnO/P3HT interface models the bottom two ZnO layers were kept fixed in order to mimic bulk ZnO.

The charge transferred from the polymer to the semiconductor was calculated as the difference $\Delta n(\mathbf{r}) = n_{\mathrm{ZnO/P3HT}}(\mathbf{r}) - [n_{\mathrm{ZnO}}(\mathbf{r}) + n_{\mathrm{P3HT}}(\mathbf{r})]$. In this expression $\mathbf{r}$ is the position vector within the computational cell, $n_{\mathrm{ZnO/P3HT}}$ is the ground-state charge density of the ZnO/P3HT interface, n_{ZnO} is the charge density of the ZnO slab without the P3HT layers in the same computational cell, and n_{P3HT} is the density of the P3HT layers without the ZnO slab. The electrostatic potential offset was calculated by integrating, using Poisson's equation, the planar average of the charge $\Delta n(\mathbf{r})$ from the middle of the ZnO slab to the middle of the P3HT layer.

As a check the electrostatic potential offset was determined by comparing the KS energy levels at the ZnO/P3HT interface, which include the effect of charge transfer, with those corresponding to the isolated ZnO and P3HT layers, which do not include the effect of charge transfer. The KS levels of the isolated components were calculated on large supercells (up to 48 Å in the direction normal to the interface) and were referred to the total local potential in vacuum. This additional calculation yielded an electrostatic potential offset of 0.53 eV. The very good agreement between these two approaches provides additional support to our results. Although both methods are expected to yield the same result, the calculation through the charge density is to be preferred because i) the density is the fundamental quantity in DFT and ii) the determination of the vacuum level through the total local potential is complicated by the electrostatic interaction between periodic replicas, and dipole corrections[58] are necessary in order to obtain accurate results.

Hybrid-Functional Calculations: Hybrid-functional calculations were performed following the approach of Alkauskas et al.[24] Accordingly, hybrid density functionals based on the Perdew, Burke, and Ernzerhof (PBE) generalized-gradient approximation to DFT,[59] in conjunction with PBE[60] pseudopotentials were used. The fraction of Hartree-Fock exchange required to reproduce the measured ZnO bandgap of 3.4 eV[61] was found to be $\alpha_s = 0.375$. In the case of P3HT, a very recent study based on photoelectron spectroscopy and inverse photoelectron spectroscopy determined an electrical gap of 2.6 eV.[41] The electrical gap is the relevant quantity for the study of the energy-level alignment and should not be confused with the optical gap of 1.9 eV,[41] which includes excitonic effects. Using the measured P3HT gap of 2.6 eV the fraction of Hartree-Fock exchange for the polymer was determined to be $\alpha_p = 0.367$. Since in the present case of a semiconductor/polymer interface the alignment of the hybrid-functional corrections to the local electrostatic potential used by Alkauskas et al.[24] is not uniquely defined, in this work the corrections were aligned directly to the Kohn-Sham eigenvalues.[62] For completeness, the hybrid-functional energy levels at the interface were also calculated by using the local electrostatic potential as a reference (i.e., the sum of the Hartree potential and the local ionic pseudopotential).[24,63] The energy levels determined by this method and the one described in the main text agreed to within 0.15 eV. This can be taken as an estimate of the error in the calculations.

Thiophene on the ZnO$(10\bar{1}0)$ *Surface*: In order to validate the method of Alkauskas et al.[24] for calculating the energy-level alignment, a small model system comprising a thiophene molecule adsorbed on the ZnO$(10\bar{1}0)$ surface was considered. In this model the thiophene molecules were arranged on the ZnO surface in a rectangular lattice of size 12.7 Å × 10.3 Å. In the optimized geometry the molecules were located such that the C atoms at the 2,5 sites of the thiophene rings were atop the ZnO dimer trenches, 2.61 Å above the surface. The energies of the VBM and CBM of ZnO, as well as the energies of the LUMO and HOMO of the molecule, were calculated using two methods: i) by extracting the Kohn-Sham DFT levels and applying hybrid-functional corrections from bulk ZnO and isolated molecule calculations (KS+ΔH scheme) and ii) by performing an explicit hybrid-functional calculation on the entire interface (H scheme). For consistency, in all the hybrid-functional calculations the same fraction $\alpha = 0.375$ of Hartree-Fock exchange was used. After setting the zero of the energy scale to the HOMO of the molecule, the following energy levels within the KS+ΔH scheme (H scheme) were obtained: thiophene LUMO 6.82 eV (6.85 eV), ZnO VBM 1.28 eV (1.25 eV), ZnO CBM 4.36 eV (4.30 eV). Therefore the energy-level alignment calculated using the KS+ΔH approach agrees with the results of a direct hybrid-functional calculation on the entire interface to within less than 0.1 eV. This very good agreement confirms the validity of the DFT+ΔH scheme. It is noted that image-charge effects[64] were not included in either scheme as these effects are not relevant to the case of the ZnO/P3HT interface considered.

Quantum Confinement in ZnO Nanowires: In hybrid organic/inorganic solar cells based on ZnO quantum dot/polymer blends[6,12–16] or ZnO nanorod/polymer interfaces,[6,7,10,16–22] the carrier confinement in the semiconductor could affect the energy-level alignment at the interface. In order to quantify this effect the difference in the bandgap between bulk ZnO and a model ZnO nanorod of diameter 1.5 nm was calculated. A model ZnO nanorod extending along the [0001] direction was generated by cutting bulk ZnO through its six $\{10\bar{1}0\}$ facets. The computational cell contained 108 atoms, the 1D Brillouin zone along the nanorod axis was sampled by means of 8 inequivalent points, and the lateral separation between adjacent periodic replicas of the nanorod was set to 10 Å. In the optimized geometry the Zn-O bond length decreased from 1.96 Å at the center of the nanorod to 1.91 Å at the surface, consistent with the requirement of local charge neutrality. The quantum confinement effect on the band gap was calculated as the variation of the DFT energy levels between bulk ZnO and the nanorod.

The band gap was found to increase from its bulk value (0.84 eV) by 0.4 eV due to quantum confinement, in agreement with previous first-principles calculations.[65] This result can be extended to nanorods of larger diameter by using a simple scaling argument based on the energy levels of an electron confined in a cylindrical well: $\Delta E_{g,2}/\Delta E_{g,1} = (d_2/d_1)^{-2}$, where d and ΔE_g represent the nanorod diameter and quantum confinement correction to the ZnO band gap, respectively. For nanorods with diameter between 8 and 100 nm[16,19,22] ΔE_g <14 meV is found, indicating that the effect of quantum confinement in ZnO on the energy-level alignment is negligible for nanorods of practical size.

Acknowledgements

The authors are grateful to A. A. R. Watt for stimulating discussions. This work is supported by the ERC under the EU FP7/ ERC grant no. 239578. Calculations were performed in part at the Oxford Supercomputing Centre. Figures involving atomic structures were rendered using VMD.[66]

This article was amended after online publication to correct an error in the display of figure 1.

Received: June 1, 2012
Published online: July 20, 2012

[1] W. U. Huynh, J. J. Dittmer, A. P. Alivisatos, *Science* **2002**, *295*, 2425.
[2] S. Günes, N. S. Sariciftci, *Inorg. Chim. Acta* **2008**, *361*, 581.
[3] J. W. P. Hsu, M. T. Lloyd, *MRS Bull.* **2010**, *35*, 422.
[4] L. Vayssieres, *Adv. Mater.* **2003**, *15*, 464.
[5] H. Sirringhaus, P. J. Brown, R. H. Friend, M. M. Nielsen, K. Bechgaard, B. M. W. Langeveld-Voss, A. J. H. Spiering, R. A. J. Janssen, E. W. Meijer, P. Herwig, D. M. de Leeuw, *Nature* **1999**, *401*, 685.
[6] P. Ravirajan, A. M Peiró, M. K. Nazeeruddin, M. Graetzel, D. D. C. Bradley, J. R. Durrant, J. Nelson, *J. Phys. Chem. B* **2006**, *110*, 7635.
[7] D. C. Olson, S. E. Shaheen, R. T. Collins, D. S. Ginley, *J. Phys. Chem. C* **2007**, *111*, 16670.
[8] D. C. Olson, S. E. Shaheen, M. S. White, W. J. Mitchell, M. F. A. M van Hest, R. T. Collins, D. S. Ginley, *Adv. Funct. Mater.* **2007**, *17*, 264.
[9] T. C. Monson, M. T. Lloyd, D. C. Olson, Y. Lee, J. W. P. Hsu, *Adv. Mater.* **2008**, *20*, 4755.
[10] D. C. Olson, Y. Lee, M. S. White, N. Kopidakis, S. E. Shaheen, D. S. Ginley, J. A. Voigt, J. W. P. Hsu, *J. Phys. Chem. C* **2008**, *112*, 9544.
[11] E. D. Spoerke, M. T. Lloyd, E. M. McCready, D. C. Olson, Y. Lee, J. W. P. Hsu, *Appl. Phys. Lett.* **2009**, *95*, 213506.
[12] W. J. E. Beek, M. M. Wienk, R. A. J. Janssen, *Adv. Funct. Mater.* **2006**, *16*, 1112.
[13] D. J. D. Moet, L. J. A. Koster, B. de Boer, P. W. M. Blom, *Chem. Mater.* **2007**, *19*, 5856.
[14] M. Wang, X. Wang, *Sol. Energy Mater. Sol. Cells* **2008**, *92*, 766.
[15] S. D. Oosterhout, M. M. Wienk, S. S. van Bavel, R. Thiedmann, L. J. A. Koster, J. Gilot, J. Loos, V. Schmidt, R. A. J. Janssen, *Nat. Mater.* **2009**, *8*, 818.
[16] J. Bouclé, H. J. Snaith, N. C. Greenham, *J. Phys. Chem. C* **2010**, *114*, 3664.
[17] D. C. Olson, J. Piris, R. T. Collins, S. E. Shaheen, D. S. Ginley, *Thin Solid Films* **2006**, *496*, 26.
[18] A. M. Peiró, P. Ravirajan, K. Govender, D. S. Boyle, P. O'Brien, D. D. C. Bradley, J. Nelson, J. R. Durrant, *J. Mater. Chem.* **2006**, *16*, 2088.
[19] L. Greene, M. Law, B. Yuhas, P. Yang, *J. Phys. Chem. C* **2007**, *111*, 18451.
[20] D. C. Olson, Y. Lee, M. S. White, N. Kopidakis, S. E. Shaheen, D. S. Ginley, J. A. Voigt, J. W. P. Hsu, *J. Phys. Chem. C* **2007**, *111*, 16640.
[21] Y. Lee, M. T. Lloyd, D. C. Olson, R. K. Grubbs, P. Lu, R. J. Davis, J. A. Voigt, J. W. P. Hsu, *J. Phys. Chem. C* **2009**, *113*, 15778.
[22] A. L. Briseno, T. W. Holcombe, A. I. Boukai, E. C. Garnett, S. W. Shelton, J. J. M. Fréchet, P. Yang, *Nano Lett.* **2010**, *10*, 334.
[23] A. A. D. T. Adikaari, D. M. N. M. Dissanayake, S. R. P. Silva, *IEEE J. Sel. Top. Quantum Electron.* **2010**, *16*, 1595.
[24] A. Alkauskas, P. Broqvist, F. Devynck, A. Pasquarello, *Phys. Rev. Lett.* **2008**, *101*, 106802.
[25] C. Woell, *Prog. Surf. Sci.* **2007**, *82*, 55.
[26] M. Goano, F. Bertazzi, M. Penna, E. Bellotti, *J. Appl. Phys.* **2007**, *102*, 083709.
[27] S. Dag, L. Wang, *Nano Lett.* **2008**, *8*, 4185.
[28] J. Northrup, *Phys. Rev. B* **2007**, *76*, 245202.
[29] A. Maillard, A. Rochefort, *Phys. Rev. B* **2009**, *79*, 115207.
[30] C. Melis, L. Colombo, A. Mattoni, *J. Phys. Chem. C* **2011**, *115*, 576.
[31] T. J. Prosa, M. J. Winokur, J. Moulton, P. Smith, A. J. Heeger, *Macromolecules* **1992**, *25*, 4364.
[32] T. J. Prosa, M. J. Winokur, R. D. McCullough, *Macromolecules* **1996**, *29*, 3654.
[33] M. Brinkmann, J. Wittmann, *Adv. Mater.* **2006**, *18*, 860.
[34] M. Brinkmann, P. Rannou, *Adv. Funct. Mater.* **2007**, *17*, 101.
[35] R. J. Kline, M. D. McGehee, M. F. Toney, *Nat. Mater.* **2006**, *5*, 222.
[36] M. I. Saba, C. Melis, L. Colombo, G. Malloci, A. Mattoni, *J. Phys. Chem. C* **2011**, *115*, 9651.
[37] T. Jirsak, J. Dvorak, J. A. Rodriguez, *J. Phys. Chem. B* **1999**, *103*, 5550.
[38] C. Caddeo, G. Malloci, G. Rignanese, L. Colombo, A. Mattoni, *J. Phys. Chem. C* **2012**, *116*, 8174.
[39] M. C. Gwinner, Y. Vaynzof, K. K. Banger, P. K. H. Ho, R. H. Friend, H. Sirringhaus, *Adv. Funct. Mater.* **2010**, *20*, 3457.
[40] M. Onoda, K. Tada, A. A. Zakhidov, K. Yoshino, *Thin Solid Films* **1998**, *331*, 76.
[41] C. Deibel, D. Mack, J. Gorenflot, A. Schöll, S. Krause, F. Reinert, D. Rauh, V. Dyakonov, *Phys. Rev. B* **2010**, *81*, 085202.
[42] H. J. Snaith, *Adv. Funct. Mater.* **2010**, *20*, 13.
[43] J.-W. van der Horst, P. A. Bobbert, M. A. J. Michels, H. Bassler, *J. Chem. Phys.* **2001**, *114*, 6950.
[44] H. Ishii, K. Sugiyama, E. Ito, K. Seki, *Adv. Mater.* **1999**, *11*, 605.
[45] X. Crispin, V. Geskin, A. Crispin, J. Cornil, R. Lazzaroni, W. R. Salaneck, J. Brédas, *J. Am. Chem. Soc.* **2002**, *124*, 8131.
[46] A. Kahn, N. Koch, W. Gao, *J. Polym. Sci., Part B: Polym. Phys.* **2003**, *41*, 2529.
[47] J. Tersoff, *Phys. Rev. B* **1984**, *30*, 4874.
[48] A. Maurano, R. Hamilton, C. G. Shuttle, A. M. Ballantyne, J. Nelson, B. O'Regan, W. Zhang, I. McCulloch, H. Azimi, M. Morana, C. J. Brabec, J. R. Durrant, *Adv. Mater.* **2010**, *22*, 4987.
[49] M. T. Lloyd, R. P. Prasankumar, M. B. Sinclair, A. C. Mayer, D. C. Olson, J. W. P. Hsu, *J. Mater. Chem.* **2009**, *19*, 4609.
[50] W. C. Tsoi, S. J. Spencer, L. Yang, A. M. Ballantyne, P. G. Nicholson, A. Turnbull, A. G. Shard, C. E. Murphy, D. D. C. Bradley, J. Nelson, J.-S. Kim, *Macromolecules* **2011**, *44*, 2944.
[51] M. W. Allen, S. M. Durbin, *App. Phys. Lett.* **2008**, *92*, 122110.
[52] P. Giannozzi, S. Baroni, N. Bonini, M. Calandra, R. Car, C. Cavazzoni, D. Ceresoli, G. L. Chiarotti, M. Cococcioni, I. Dabo, A. Dal Corso, S. de Gironcoli, S. Fabris, G. Fratesi, R. Gebauer, U. Gerstmann, C. Gougoussis, A. Kokalj, M. Lazzeri, L. Martin-Samos, N. Marzari,

F. Mauri, R. Mazzarello, S. Paolini, A. Pasquarello, L. Paulatto, C. Sbraccia, S. Scandolo, G. Sclauzero, A. P. Seitsonen, A. Smogunov, P. Umari, R. M. Wentzcovitch, *J. Phys.: Condens. Matter* **2009**, *21*, 395502.
[53] D. Vanderbilt, *Phys. Rev. B* **1990**, *41*, 7892.
[54] N. Troullier, J. L. Martins, *Phys. Rev. B* **1991**, *43*, 1993.
[55] M. Fuchs, M. Scheffler, *Comput. Phys. Commun.* **1999**, *119*, 119.
[56] D. M. Ceperley, B. J. Alder, *Phys. Rev. Lett.* **1980**, *45*, 566.
[57] J. P. Perdew, A. Zunger, *Phys. Rev. B* **1981**, *23*, 5048.
[58] L. Bengtsson, *Phys. Rev. B* **1999**, *59*, 12301.
[59] J. P. Perdew, M. Ernzerhof, K. Burke, *J. Chem. Phys.* **1996**, *105*, 9982.
[60] J. P. Perdew, K. Burke, M. Ernzerhof, *Phys. Rev. Lett.* **1996**, *77*, 3865.
[61] A. Mang, K. Reimann, S. Ruebenacke, *Solid State Commun.* **1995**, *94*, 251.
[62] F. Giustino, A. Pasquarello, *Surf. Sci.* **2005**, *586*, 183.
[63] C. G. Van de Walle, R. M. Martin, *Phys. Rev. B* **1987**, *35*, 8154.
[64] J. B. Neaton, M. S. Hybertsen, S. G. Louie, *Phys. Rev. Lett.* **2006**, *97*, 216405.
[65] H. J. Xiang, J. Yang, J. G. Hou, Q. Zhu, *Appl. Phys. Lett.* **2006**, *89*, 223111.
[66] W. Humphrey, A. Dalke, K. Schulten, *J. Mol. Graphics* **1996**, *14*, 33.